AIChE

Ab Initio Energy Calculations and Macroscopic Rate Modeling of Hydroformylation of Higher Alkenes by Rh-Based Catalyst

Maizatul S. Shaharun, Binay K. Dutta, and Hilmi Mukhtar
Dept. of Chemical Engineering, Universiti Teknologi Petronas, Bandar Seri Iskandar, 31750 Tronoh, Perak, Malaysia

DOI 10.1002/aic.11936
Published online August 24, 2009 in Wiley InterScience (www.interscience.wiley.com).

Ab initio quantum chemical computations have been done to determine the energetics and reaction pathways of hydroformylation of higher alkenes using a rhodium complex homogeneous catalyst. Calculation of fragments of the potential energy surfaces of the $HRh(CO)(PPh_3)_3$-catalyzed hydroformylation of 1-decene, 1-dodecene, and styrene were performed by the restricted Hartree-Fock method at the second-order MØller-Plesset (MP2) level of perturbation theory and basis set of 6-31++G(d,p). Geometrically optimized structures of the intermediates and transition states were identified. Three generalized rate models were developed on the basis of above reaction path analysis as well as experimental findings reported in the literature. The kinetic and equilibrium parameters of the models were estimated by nonlinear least square regression of available literature data. The model based on H_2-oxidative addition fitted the data best; it predicts the conversion of all the alkenes quite satisfactorily with an average deviation of 7.6% and a maximum deviation of 13%. © 2009 American Institute of Chemical Engineers *AIChE J,* 55: 3221–3233, 2009

Keywords: ab initio computation, quantum chemical calculation, hydroformylation, kinetic modeling, higher olefins, homogeneous catalysis

Introduction

Molecular modeling based on quantum mechanical computations is emerging as a useful and reliable strategy of predicting energetics and kinetics of chemical reactions.[1,2] The strategy has three major ramifications, the ab initio electronic structure and molecular orbital (MO) calculations, semiempirical methods, and molecular mechanics. Of the three, ab initio molecular orbital methods are the most accurate and consistent because they provide the best mathematical approximation to the actual system.[3] The term ab initio implies that the computations are based on the laws of quantum mechanics, the masses and charges of the electrons and atomic nuclei, and the values of fundamental physical constants. Virtually, no conceptual approximations are involved.[4] Molecular orbital methods deal with solution of the Schrodinger's equation for a chemical system using a "basis set" of functions that satisfy a series of rigorous mathematical approximations. Ab initio molecular orbital calculations are specified by a "model chemistry."[4] The accuracy and computational time depend upon the choice of the method and the basis set, the general structure and electronic state of the molecular system under study (e.g., charge and spin states), and the treatment of electron spin. Reasonable accuracy in moderate computer time may be achieved for larger molecules ($n \sim$ 10–30 atoms) only by using the basic theory with minimal basis sets (i.e., H-F or Hartree-Fock approximation), whereas calculations on chemical reactions between simple diatomic molecules can be performed with the state-of-the-art model chemistries. For very large

Additional Supporting Information may be found in the online version of this article.

Correspondence concerning this article should be addressed to B. K. Dutta at bdutta@pi.ac.ae
Current address of B. K. Dutta is the Petroleum Institute, Abu Dhabi, UAE.

systems ($n \sim 50$ atoms or more), an excessive computational time may be avoided with less sophisticated models, like semi-empirical methods and molecular mechanics.[5]

In course of our work on kinetic studies of hydroformylation of higher alkenes in a thermomorphic solvent system,[6] we came across only few recent publications on ab initio calculation of energetics of hydroformylation of lower alkenes with a view to identifying the reaction pathways, the transition states, and eventually to develop a useful rate equation. On the other hand, a pretty large number of papers appeared during the last 3 decades on macroscopic and empirical kinetic modeling of the rate of hydroformylation of both lower and higher alkenes (a brief account of these work will be given later). This prompted us to explore the application of the ab initio computational technique to the commercially important hydroformylation reaction of higher alkenes and to compare the results with macroscopic experimental data already available in the literature.

Hydroformylation is the reaction process of an olefin with syngas (H_2/CO) in the presence of cobalt, rhodium, or platinum catalyst to produce an aldehyde that may have a wide range of applications in plasticizers, detergents, perfumes, fragrances, surfactants, etc.[7–9] Although the actual steps of the homogeneous catalytic gas–liquid reaction are complex, the overall reaction can be represented by Eq. 1.

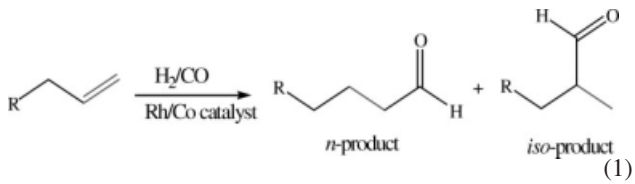

(1)

The most widely used ligand in a homogeneous hydroformylation process is triphenylphosphine (PPh_3). In the rhodium-PPh_3 catalyzed hydroformylation, it has been established that hydridocarbonyl-tris(triphenylphosphine)rhodium (I) ($HRh(CO)(PPh_3)_3$) is a direct catalyst precursor. The mechanism of the previous generation cobalt-catalyzed hydroformylation as postulated by Heck and Breslow[8] has been found to explain the action of phosphine-modified rhodium carbonyl as well.[10,11] In spite of the commercial importance of the rhodium-PPh_3 catalyst, only limited data have been published on the kinetics of the hydroformylation reaction under the industrial operating conditions (T = 343–393 K, CO partial pressure = 5–25 bar, H_2 partial pressure = 5–25 bar, Rh loading ~1 mM and alkene concentration = 0.1–2 M). Here we have applied the ab initio technique of quantum chemical computation to obtain the energetics and to identify the reaction pathways of Rh-catalyzed hydroformylation of higher alkenes (1-octene, 1-decene, 1-dodecene, and styrene) using low concentrations of phosphine ligand. Because the available computational tools did not allow prediction of the kinetic parameters of the systems under study, we have developed generalized macroscopic reaction rate equations based on the mechanism and pathways given by the ab initio calculation. The kinetic constants were evaluated by fitting experimental hydroformylation data at different process conditions. The resulting activation energies matched remarkably well with that predicted by the quantum chemical method thereby validating its applicability to this class of homogeneous catalytic reactions.

The ab initio molecular orbital calculation

The quantum mechanical description of chemical bonds is given by a space and time dependent probability distribution: the molecular wavefunction, $\Psi_{mol}(t)$, defined by the Schrödinger equation

$$\hat{H}_{mol}\Psi_{mol}(t) = i\hbar\frac{\partial\Psi_{mol}(t)}{\partial t} \tag{2}$$

where $\hat{H}$ is the Hamiltonian operator representing the sum of kinetic and potential energies, $\hbar$ is Planck's constant, i is the imaginary unit, and t is time. For systems of more than two interacting particles, the Schrödinger equation cannot be solved exactly. Therefore, all ab initio calculations for molecules involve some level of approximation and indeed, some level of empirical parameterization. The standard MO treatment for most closed-shell molecules involves a spin-restricted Hartree-Fock self-consistent field (HF-SCF) calculation. HF-SCF calculations generally yield accurate molecular structures but are less successful in predicting molecular energies. The main source of error in HF calculations is neglect of electron correlation, which results in systematic overestimates of molecular energies. Different tools of varying complexities have been developed to enhance the accuracy of computation.[12,13]

Ab initio MO studies require a basis set of mathematical functions to solve the wave equation. Standard ab initio software packages provide a choice of basis sets that vary both in size and in their description of the electrons in different orbitals. Quantitative accuracy improves with the size of basis sets, because larger basis sets contain more adjustable parameters and thus offer better approximations of the true molecular wave functions. In general, ab initio MO studies on complex systems should begin with calculations using small basis sets, to obtain a qualitative assessment of molecular properties. For general use, the smallest standard basis set is recommended in the Gaussian 98 is 6-31G(d) package. A number of quantities such as molecular orbital energies, total energy from electronic and nuclear repulsion, heat of formation, and dipole moment are obtainable from molecular orbital calculations.

It will be pertinent at this point to refer to the reported applications of the methodology to the study of energetics and kinetics of noncatalytic and catalytic reactions, both homogeneous and heterogeneous. Saeys et al.[1] developed a Langmuir-Hinshelwood-Hougen-Watson (LHHW) kinetic model for the hydrogenation of toluene over Pt catalyst based on the first-principles density functional theory calculations. The LHHW model is able to capture the main trends in the reaction pathways and rates. Rocha et al.[14] performed a theoretical study on the homogeneous catalysis of isomerization of β-pinene, a hydroformylation perecursor. The isomerization was investigated at three different levels of theory—HF, MP2, and MP4(SDQ)—using four different sizes of basis set, namely, 6-31G, 6-31G(d), 6-31+G(d), and 6-311++G(d,p), provided in the computational package. It was reported that the use of different basis set and the inclusion of the electron correlation effects had little influence on the relative stability of the β-pinene isomers but the effect on the energy barrier for the isomerization reaction was

significant. Another theoretical study on the mechanism of the isomerization of 1-butene catalyzed by Rh-complex has been reported by Luo et al.[15] The quantum mechanical calculations were carried out in the density functional theory framework to evaluate the potential energy profile and the reaction mechanisms involved. Rocha[16] studied the reaction mechanisms involved in the last step of the catalytic cycle of the hydroformylation of an alkene promoted by Pt-Sn catalyst, which is a hydrogenolysis process. Very recently, Cavallotti et al.[2] reported ab initio computational studies on cyclohexane oxidation leading to kinetic parameters of primary reactions. These results together with available experimental data were used to formulate and test a detailed kinetic model.

The quantum chemical calculation of the potential energy of intermediates and transition states requires a reaction scheme to begin the process. In this way, the outline of a kinetic model with a sound theoretical basis is built which can be used to predict the macroscopic parameters of the process and to compare directly with experiment (a kind of benchmarking). In some cases, it may be possible to predict the outcome of new chemical processes.

Computational strategy

A tentative mechanism of the reaction pathways is a prerequisite of the ab initio computation.[17] The quantum-chemical calculations were performed with the GAMESS Pro 11.0 program package and ChemBio3D 11.0 as a front end graphical user interface (GUI). Geometries of all the transition states as well as of the intermediates were optimized at the restricted Hartree-Fock (RHF)/6-31G(d,p) level. For the energetics, the electron correlation calculations were performed with the frozen-core second-order Møller-Plesset (MP2) perturbation method, using basis sets 6-31++G(d,p).[15] We used two basis sets, basis set I for the RHF geometrical optimization and basis set II for the MP2 energy calculation and higher level calculations. The vibrational analysis and internal reaction calculations (IRC) were also performed to verify the transition states. Vibrational frequencies were calculated at the RHF/6-31G(d,p) level. A scaling factor of 0.937 was used.[18] In addition, zero point energy (ZPE), which a quantum system possesses at 0 K in contrast to a classical system, was also calculated. The contribution of the ZPE that arises out of the residual vibration, to the reaction enthalpy and Gibbs free energy may sometimes be significant. Because ab initio ZPE calculations yield slightly higher values than actual, a scaling factor of 0.89 was used.[19] The contribution of ZPE to the PE was within 5% for most of the species involved in this study.

To check the accuracy of our computational strategy and methodology, we performed test calculations of an intermediate (Coutinho et al.[20] called it μ-acyl complex) identified in the process of hydroformylation of phosphino-butene with a hetero-bimetallic complex catalyst.[20] We have confirmed that the structure of the complex calculated at MP-2/6-31G(d,p) level is in good agreement with that experimentally determined by Coutinho et al. using X-ray crystallography and theoretically calculated latter on by Tang et al.[21] The transition state structures of the species in the present study were located on the potential energy surface using the quadratic synchronous approach of Schlegel and Yarkony,[17] starting with a low level computed Hessian matrix for a suitable guess of transition state structure. Calculation of the harmonic vibrational frequencies for the transition state (TS) species revealed that each contained the single imaginary frequency required to classify it as a true TS. Activation energies were calculated for the five transition structures of Rh-catalyzed hydroformylation of ethylene identified by Matsubara et al.[22] (alkene insertion, H-insertion onto alkene ligand, CO insertion, H_2 oxidative addition, and aldehyde reductive elimination). However, only three transition states with the three highest energy barrier (alkene insertion, CO insertion, and H_2 oxidative addition) were selected for detailed study in our work. Structure of PH_3 is chosen to mimic the organic phosphorus ligand PPh_3, to avoid excessive computational time without any appreciable loss of accuracy.[15,23]

The reaction pathways

The tentative reaction pathways for ab initio computation is shown in Figure 1 (computations are confined to the reactions within the dotted box). The pathways and the species involved in various stages are discussed in Table 1. Qualitative reasoning and some available experimental observations form the basis of the scheme. According to van Leeuwen et al.,[10] hydroformylation reactions are quite sensitive to experimental conditions such as the concentrations of the catalyst, carbon monoxide, hydrogen, the olefin, and the added ligand. At low Rh concentration, using $HRh(PPh_3)_3CO$ as the catalyst precursor without addition of excess PPh_3 ligands, substantial dissociation can occur with the formation of mono-phosphine or phosphine-free catalysts. Therefore, it is anticipated that at a high CO pressure of 20–40 bar and low PPh_3 concentration, the PPh_3 ligand of the complex $HRh(PPh_3)_3CO$ (which is the catalyst precursor, **A**) can exchange with carbon monoxide to form **B** and **C**(Figure 1). The ^{31}P NMR magnetization transfer experiments described by Brown and Kent[24] also indicated that PPh_3 dissociation from the RhL_2 [the complex **B**; **L** = ligand] complex could occur at a significantly slower rate than the corresponding PPh_3 dissociation from tris-triphenylphosphine complex, A. In addition, spectroscopic experiments have revealed that under hydroformylation conditions, rhodium tri(*o-tert*-butylphenyl)phosphite complex is coordinated by only one phosphite, $HRh[P(OAr)_3](CO)_3$.[25] van der Veen et al.[26] claimed that the rate of hydroformylation is two orders of magnitude slower than the rate of carbon monoxide exchange of isomers of type **B**. The relative concentrations of these intermediates are controlled by the PPh_3 and CO concentrations. Thus, we may conclude that the initiation of the catalytic cycle by dissociation of CO and PPh_3 should not be rate determining because it has been found to be fast on the time-scale of hydroformylation.

Wilkinson suggested that species C, formed at a low concentration of PPh_3, leads to a lower selectivity for linear aldehyde (linear:branched = 4:1) when compared with hydroformylation reaction with additional amount of PPh_3.[27] The overall steric hindrance at the rhodium metal of species **B** is low because two relatively small carbonyl ligands are coordinated next to two bulky triphenylphosphine, PPh_3. The

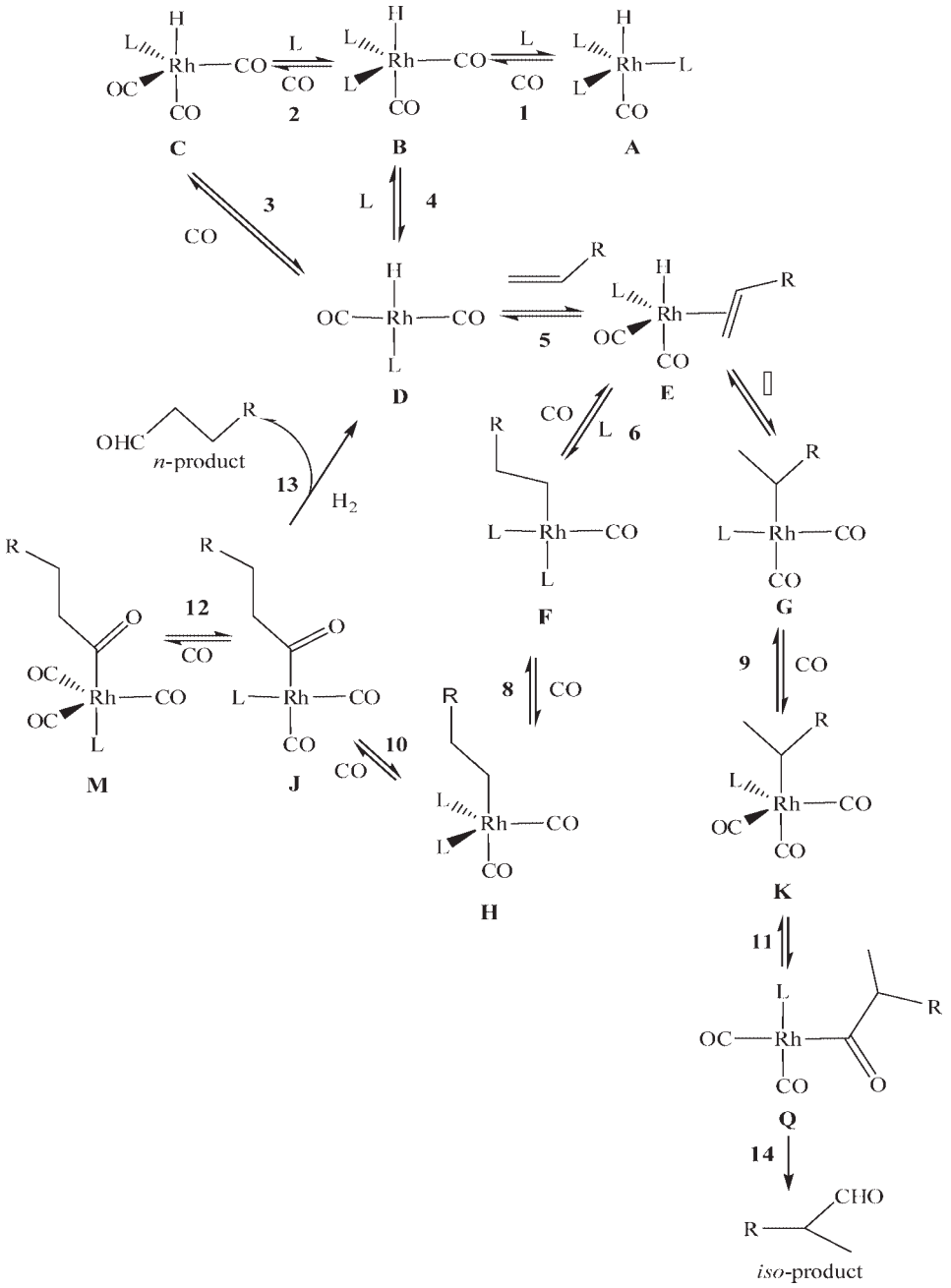

Figure 1. Plausible steps for rhodium catalyzed hydroformylation in the presence of low concentration of phosphine ligand.

rhodium center containing two weak phosphine donors and strongly electron withdrawing carbonyl ligands is predictably electron deficient. As a result, the carbonyl ligands are strongly bound and the fast dissociation of phosphine (structure **C**) and subsequent olefin addition results in high reaction rates. Hydride migration in a latter step results in the formation of the linear or branched rhodium alkyl complex, **F** and **G** (Figure 1).

The isomerization reaction is often ignored in developing the rate equation. Under the reaction condition, the rhodium alkyl complexes **F** and **G** can undergo either migratory insertion forming the rhodium acyl complex or β-hydride elimination. As for the primary rhodium alkyl **F**, the β-hydride elimination will lead to the initial substrate. However the secondary rhodium alkyl complex, **G** can lead to the 1-alkene and a by-product, internal 2-alkenes, by β-hydride elimination. Because β-hydride elimination is faster for the secondary rhodium alkyl than for the primary rhodium alkyl complex, high isomerization rates will reduce the formation of the branched rhodium acyl to a larger extent than the linear rhodium acyl. Another possible side reaction is the formation of the inactive tricarbonyl rhodium

Table 1. Description of the Catalytic Cycle in Figure 1

Step	Description
1	For PPh_3 as the ligand (L), the starting complex is $HRh(CO)(PPh_3)_3$ (complex **A**), which in the presence of carbon monoxide forms diphosphine intermediate, containing the phosphine ligands in equatorial positions (ee) or one in an apical position and the other ligand in an equatorial position (ae). Brown and Kent[20] found a preference for the "ee" isomer (i.e., complex **B**). The other possible isomer (ae) of the complex is not shown.
2	At low Rh concentration, using $HRh(CO)(PPh_3)_3$ as the precursor without addition of PPh_3 ligand, substantial dissociation will occur to form monophosphine catalyst, complex **C**.[10] In addition, according to Jongsma et al.,[21] complex **B** may undergoes exchange of ligand to form single coordinated PPh_3 ligand, **C**, at high CO pressure.
3 and 4	Revesible addition/elimination of either **L** or CO from **B** or **C** leads to the square-planar intermediate **D**.
5	Complex **D** associate with olefin to give complex **E** which eventually gives rise to the product aldehyde (*n*- or *iso*-) through a number of stpes that follow.
6 and 7	Complex **E** undergoes a migratory insertion step to give square planar alkyl complexes **F** or **G**. Complex **E** can undergo β-hydride elimination, thus leading to isomerization especially when higher alkenes are used (step 7). Wilkinson[10] suggested that formation of species **F**, lead to higher linear aldehyde selectivity (*n*:*iso* = 20:1), and that species G, containing only one phosphine, lead to a lower selectivity for linear aldehyde (*n*:*iso* = 4:1).
8 and 9	Complex **F** (and also **G**) react further with CO to form trigonal bypiramidal complexes **H** (and also **K**).
10 and 11	Complex **H** (and also **K**) undergoes the second migratory insertion of the alkyl ligand to form acyl complexes **J** (and also **Q**).
12	Complex **J** can react further with CO to give the saturated acyl intermediate **M**, which have been observed spectroscopically.[20]
13 and 14	Complex **J** (and **Q**) reacts with H_2 to give the aldehyde product and gives back the unsaturated intermediate **D**. The reaction with H_2 involves presumably oxidative addition and reductive elimination.

species **M**, from the addition of CO to the unsaturated rhodium acyl complex, **J**.[23,28] Further details of the reaction pathways are given in Table 1.

Results and Discussion

Quantum chemical calculation

As stated before, quantum chemical calculations are confined to the reactions within the dashed box in Figure 1. The main reaction mechanism involves nine elementary steps (besides other secondary steps leading to the iso-product), three of which pass through transition states (TS): (i) alkene insertion (step 5), (ii) formation of acyl complex (step 10), (iii) H_2 oxidative addition (step 13). These three reactions will be examined individually, and at the end the overall potential energy profile will be analyzed. Figures 2a–c show the optimized structures of the three transition states. The computed potential energies of the various species appearing in the proposed reaction pathways (Figure 1) are shown in Figures 3a–c against the reaction coordinate. The reaction coordinate represents the progress along the reaction pathways. It is expedient to mention here that two intermediate species, which are called **N** and **P**, appear between **J** and the product aldehyde during the potential energy calculation. These are a dihydride acyl species and an aldehyde coordinated intermediate, respectively. However, because the transition state involving aldehyde reductive elimination was not selected for detailed study in this work, the species **N** and **P** are not included in the catalytic cycle in Figure 1.

Alkene insertion

An alkene ligand attaches to the catalyst molecule in this step. This is followed by insertion or integration of the alkene into the Rh-H bond to generate a saturated Rh-alkyl complex **F** (or **G**). The HF optimized geometry of the alkene insertion transition state **TS1** originating from H_2-alkene adduct **E1** is displayed in Figure 2a. In proceeding from the H_2-alkene adduct to the insertion transition state,

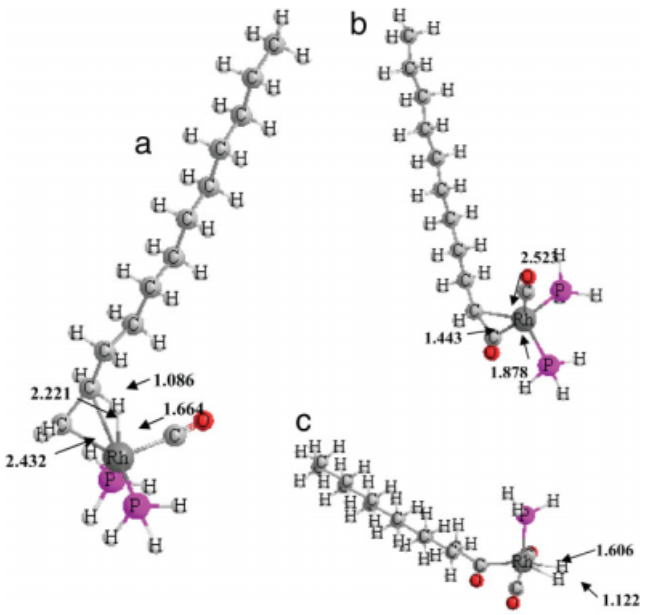

Figure 2. (a) Selected geometrical parameters of optimized structures (Å) of the transition state TS-1 (E1/F1) for the 1-dodecene insertion at RHF level; (b) Optimized bond lengths (Å) of transition state TS-2 (H1/J1) for the CO insertion at the RHF level (1-octene); (c) Optimized structures (Å) of the transition state TS-3 (J1/N1) for the H_2 oxidative addition at the RHF level (1-dodecene).

[Color figure can be viewed in the online issue, which is available at www.interscience.wiley.com.]

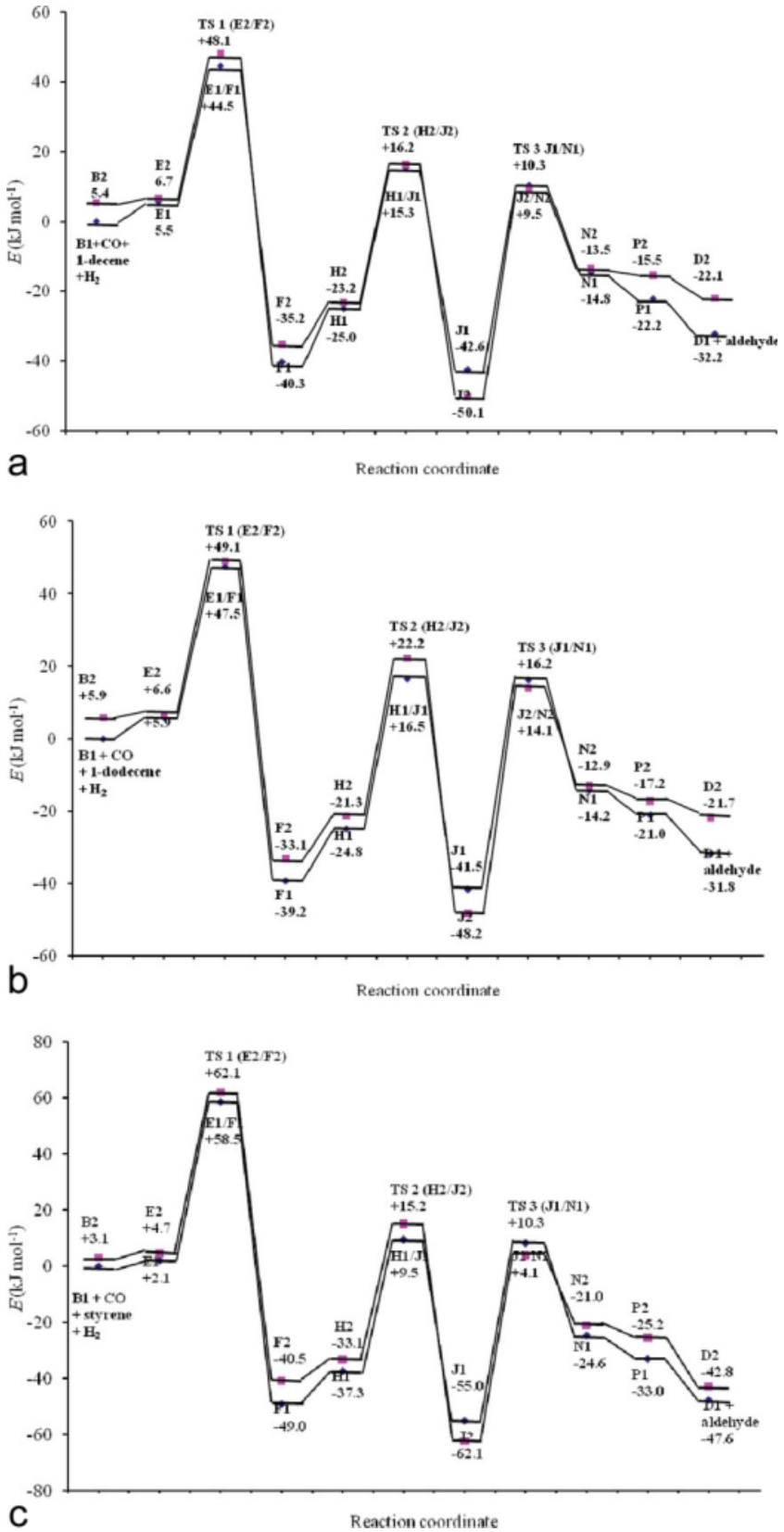

Figure 3. (a) The potential energy profile of 1-decene hydroformylation reaction (the "ee" isomer is denoted by "1" and the "ae" isomer by "2"); (b) The potential energy profile of 1-dodecene hydroformylation reaction; (c) The potential energy profile of styrene hydroformylation reaction.

[Color figure can be viewed in the online issue, which is available at www.interscience.wiley.com.]

the alkene ligand must rotate out of the equatorial plane and shift upward in order to facilitate its alkene group to align with the axial hydride. As it can be seen in Figure 2a, the alkene ligand in the transition state oriented itself intermediary between a perpendicular and a parallel alignment. Simultaneously, the axial hydride bends toward the incoming alkene ligand. In fact, two alkene insertion transition states **TS1(E1/F1)** and **TS1(E2/F2)** were identified at the MP2 level: the former was due to the "ee" H_2-alkene adduct, whereas the latter originated from "ae" H_2-alkene adduct. Harmonic vibrational frequency calculations confirmed that both the species are indeed transition states containing a single imaginary frequency. The structures of **TS1(E1/F1)** and **TS1(E2/F2)** could be further confirmed by calculation of the IRC, **TS1(E1/F1)** generated the trans-Rh-alkyl insertion product (**F1**), while **TS1(E2/F2)** led to the cis-Rh-alkyl insertion product (**F2**). The activation energy barrier varies from 39 to 57.4 kJ mol^{-1} for the three alkenes at the MP2 level, depending upon the size of the alkene molecule. This activation energy is required for the deformation of trigonal-bypiramidal structure as well as to meet the energy demand for bond exchange in olefin insertion.

Formation of acyl complex

Along the reaction coordinate, the axial alkyl ligand is bent toward the equatorial CO ligand before the three-member ringed, trigonal bypyramidal-like transition structure was formed (Figure 2b). This distortion was coupled with a bending of the oxygen atom of the CO ligand away from the incoming alkyl group in order to reduce the steric and electronic repulsion. The bond angle Rh—C—O changes from 178° in **H2** to 163° in TS2(H2/**J2**) which indicated that the CO ligand also bent slightly to align with the incoming alkyl ligand. The product of CO insertion had two isomers, **J1** and **J2**. Obviously, **J2** is a more stable isomer by a preferred energy in the range of 6.7–7.5 kJ mol^{-1} of **J1**. All these were confirmed by IRC calculations.

H_2 oxidative addition

The third transition state (Figure 2c) considered in this work was oxidative addition of H_2 to the unsaturated four-coordinated complexes **J** to give rise to a dihydride acyl species **N** (Figure 3). Calculated at the MP2 level, the H_2 addition step for all three substrates was predicted to be endothermic to the extent of 21.0–37.5 kJ mol^{-1}. We can visualize two alternative ways of attack by a reacting hydrogen molecule: (i) the H_2 molecule collides with the central Rh parallel to **L**—Rh—C(CO) in the species **J** forming transition state **TS3(J1/N1)**, and (ii) it does so along the C(CO)—Rh—C(CO) line and moves up to rhodium yielding **TS3(J2/N2)**. The transition states give rise to oxidative addition products **N1** and **N2**, respectively. Calculated at MP2 level of theory, the energy barrier for TS 3(**J2/N2**) was a little lower than the alternative pathway through TS3(**J1/N1**). Thus the reaction with H_2 attack along C(CO)—Rh—C(CO) can be regarded as the more feasible one of the two alternative paths. Calculation using 1-octene, 1-dodecene, and styrene as substrate, the energy barrier for the two paths was in the range of 52.9–66.2 kJ mol^{-1}.

Table 2. Activation Energy (kJ mol^{-1}) for the Transition States Calculated at MP2 Level of Theory

	Activation Energy (kJ mol^{-1})					
	Alkene Insertion		Acyl Complex Formation		H_2 Oxidative Addition	
Substrate	ee (1)	ae (2)	ee (1)	ae (2)	ee (1)	ae (2)
1-Decene	39.0	41.4	39.4	40.3	52.9	59.6
1-Dodecene	41.6	42.5	43.5	41.0	57.7	62.3
Styrene	56.4	57.4	48.3	46.8	63.2	66.2

ee, both ligands in equatorial positions (alternative notation used in Fig. 3: "1"); ae, one ligand in apical and the other in equatorial position (alternative notation used in Fig. 3: "2").

The activation energies for the above three reaction steps of the alkenes were obtained from the potential energy values calculated by considering higher electron spin number (triplet). It may be mentioned that use of this higher spin number yielded more consistent values of the potential energy when compared with those obtained by using the spin number 1 in our initial calculations. The tabulated values (Table 2) show that if both the coordinating groups (**L**, CO) are in equatorial positions (ee), the activation energy is generally less than that for the case of one ligand in apical and the other in equatorial (ae) positions. The variations in the activation energies for the transition states of the three alkenes can be explained in terms of steric hindrance or steric crowding of the alkyl ligands.[29] Styrene, which has a bulky phenyl group, has the highest activation energy among the three olefins for all the transition states. The activation energy of the reactions of 1-dodecene is higher than the corresponding value of 1-decene and can be explained on the same basis. *X-Y-Z* structures of the species at stationary points as well as the vibrational frequencies are provided in the Supporting Information File.

The potential energy profile

The potential energy profile of the hydroformylation of 1-decene, 1-dodecene, and styrene are presented in Figures 3a–c respectively. The active catalyst, which mediates the catalytic cycle, is considered to be $HRh(CO)_2(PPh_3)_2$ [**B** in Figure 1]. The transition state of the insertion of alkene into Rh-complex (**TS-1**), formation of acyl complex (**TS-2**), and oxidative addition of H_2 (**TS-3**) were optimized by the ab initio MO method to determine the potential energy surface of the intermediates. The H_2 oxidative addition (**TS-3**) was found to be endothermic, and the alkene insertion (**TS-1**) and CO insertion reaction (**TS-2**) are exothermic. Similar results were reported for the hydroformylation of ethene by Musaev et al.[23] The largest barrier is the H_2 oxidative addition step, in agreement with the experimental proposal that the H_2 oxidative addition is rate determining.

The potential energy diagrams Figures 3a–c deserve further explanation in relation to the species considered in the reaction pathways (Figure 1). The transition state **TS2** (**H1/**

J1) for the "ee" isomer and **H2**/**J2** for the "ae" for the acyl complex formation were obtained by Intrinsic Reaction Coordinate (IRC) calculation at MP2 level. It was found that **TS2** (**H1**/**J1**) originated from the **H1**(ee) and generated the trans-Rh-acyl insertion product (**J1**). Similarly, the cis-Rh-acyl insertion product (**J2**) resulted from the **H2** (ae) species. Possible formation of isomers was taken into account in potential energy calculations. The equilibrium geometries of each species were first determined by optimizing the structures by ab initio RHF method using a 6-31G(d,p) basis set. A conformational analysis was carried out on the optimized geometries (ae or ee geometric isomers) by rotating the torsional angles of the ligands in steps of 30°. The resulting conformers (a total of about 100) were further optimized by energy minimization. A conformer was retained if its energy varied by less than 2 kJ mol^{-1} from that of the most stable conformer. Thus, only the most stable conformers with lowest energy was selected.

The macroscopic rate equation

Kinetics of industrially important hydroformylation of higher alkenes have been reported by several workers. In particular, the kinetics of homogeneous hydroformylation of higher alkenes using Rh-based catalyst have been studied by Palo and Erkey,[30] Bhanage et al.,[31] Divekar et al.,[32] and Deshpande and Chaudari.[33] However, the rate equations proposed were essentially empirical. Palo and Erkey[30] studied the kinetics of hydroformylation of 1-octene in supercritical carbon dioxide ($scCO_2$) with $HRh(CO)[P(p\text{-}CF_3C_6H_4)_3]_3$ at 50°C and 273 bar. The observed kinetic behavior differs from the conventional systems using $HRh(CO)(PPh_3)_3$ in organic solvents. The most significant observations reported by Palo and Erkey[30] are the 0.5 order rate dependence on $[H_2]$, the lack of substrate inhibition, and the absence of a critical catalyst concentration. This may be due to several factors: $scCO_2$ solvent effects, the modified phosphine ligands, and the increased H_2 and CO concentrations relative to conventional systems. Chaudari and coworkers[31–33] developed kinetic rate expressions using several different substrates (1-hexene, 1-decene, and 1-dodecene in organic solvents) and calculated the rate parameters and activation energy for each system. A mechanistic model was also proposed for the hydroformylation of styrene by Nair et al.[28] but was not used to develop a general kinetic equation for the hydroformylation of olefins. Summarizing the observations reported in the literature, it can be stated that the rate of hydroformylation has been found to be influenced positively by increasing the concentration of catalyst and hydrogen, whereas increased carbon monoxide exhibited a negative effect. The apparent activation energy required for aldehyde formation has been found to be in the range of 30–100 kJ mol^{-1}.

We have developed mechanistic, macroscopic rate equations (we call it "macroscopic" in order to differentiate it from the quantum chemical approach) for higher alkenes based on the reaction pathways depicted in Figure 1 using the conventional quasi-steady state formalism. It is assumed that (i) all but one of the reaction steps are in equilibrium, (ii) the starting intermediate species at the reaction interface is the complex $HRh(CO)_2(L)_2$, and (iii) the total rhodium concentration remains constant. Three rate equations have been developed corresponding to the three transition states identified by quantum chemical calculations. The following reaction steps (Figure 1) are considered.

$$B + CO \Leftrightarrow C \tag{3i}$$

$$C \Leftrightarrow D + CO \tag{3ii}$$

$$B \Leftrightarrow D \tag{3iii}$$

$$D + RCH{=}CH_2 \Leftrightarrow F + CO \tag{3iv}$$

$$D + RCH{=}CH_2 \Leftrightarrow G \tag{3v}$$

$$F + CO \Leftrightarrow J \tag{3vi}$$

$$J + H_2 \rightarrow RCH_2CH_2CHO + D \tag{3vii}$$

$$J + CO \Leftrightarrow M \tag{3viii}$$

Also, the following expressions for the concentrations of the different intermediates can be written in terms of the equilibrium constants of the reactions.

$$[B] = \frac{[J]}{K_1K_2K_4K_6[\text{alkene}]}; \quad [C] = \frac{[J][CO]}{K_2K_4K_6[\text{alkene}]};$$
$$[D] = \frac{[J]}{K_4K_6[\text{alkene}]}; \quad [F] = \frac{[J]}{K_6[CO]};$$
$$[G] = \frac{K_5[J]}{K_4K_6}; \quad [K] = K_8[J][CO]$$

If the H_2 oxidative addition is rate-controlling, the rate of reaction is given by [see Eq. 3(vii)]

$$\text{Rate} = k\,[J]\,[H_2]. \text{ (where } k \text{ is the rate constant)} \tag{4}$$

An expression for the concentration of the species [J] can be obtained from a total catalyst balance at steady state.

$$[\text{Catalyst}] = [B] + [C] + [D] + [F] + [G] + [J] + [M] \tag{5}$$

And the rate equation can be written as Model M1:

$$\text{Rate} = \frac{k[\text{catalyst}][CO][\text{alkene}][H_2]}{1 + K_1^*[CO] + K_2^*[CO]^2 + K_3^*[\text{alkene}] + K_4^*[CO][\text{alkene}] + K_5^*[CO]^2[\text{alkene}]} \tag{6}$$

where K_1^*–K_5^* are constants derived from the equilibrium constants of the individual reactions. This equation is similar in form to the empirical model proposed by Bhanage et al.,[31] Divekar et al.,[32] and Deshpande and Chaudari.[33]

The second kinetic model (M2) was proposed considering the migration insertion of the alkene into the Rh—H bond, and the rate limiting step is Eq. 3(iv). The corresponding rate equation can be derived in the form (Model M2),

$$\text{Rate} = \frac{k[\text{catalyst}][\text{CO}][\text{alkene}]}{\left(1 + +K_1^*[\text{CO}] + K_2^*[\text{alkene}] + K_3^*[\text{CO}][\text{alkene}] + K_4^*[\text{CO}]^2[\text{alkene}]\right)} \tag{7}$$

Similarly, considering the formation of the acyl complex is rate-controlling, we get Model M3,

$$\text{Rate} = \frac{k[\text{catalyst}][\text{CO}][\text{alkene}][\text{H}_2]}{1 + K_1^*[\text{CO}] + K_2^*[\text{CO}]^2 + K_3^*[\text{alkene}] + K_4^*[\text{CO}][\text{alkene}] + K_5^*[\text{H}_2]} \tag{8}$$

We call the models M1, M2, and M3 ''generalized models'' corresponding to the three rate determining steps indicated by the quantum calculations and are independent of any particular alkene. The proposed rate equation (M1) is only consistent with the experimental observations, indicating a first-order dependence on [H_2] and [catalyst], first order in CO at low pressure and negative order at high pressures, and fractional order in olefin concentration. The negative order with respect to CO concentration at high pressure may be explained by the accumulation of species K, which are outside of the cycle under these conditions and therefore should inhibit the rate of the reaction.[34]

The rate parameters

Experimental hydroformylation rate data extracted from the published literature were used to evaluate the kinetic and equilibrium constants (k and K's) of each of the three 1-alkenes. The data sources and the ranges of the process parameters (pressure, concentration, temperature) are listed in Table 3. The $HRh(CO)(PPh_3)_3$ catalyst in an organic solvent was used for the alkene substrates except for 1-octene for which $HRh(CO)[P(p\text{-}CF_3C_6H_4)_3]_3$ was used as catalyst in supercritical carbon dioxide ($scCO_2$) solvent. Because no side reactions were reported by the researchers[28,31,32] under the stated experimental conditions, the rate data represented the overall hydroformylation of an alkene to the corresponding aldehyde.

Nonlinear least square regression based on the criterion of minimization of the mean residual sum of squares (MRSS) was performed to determine the kinetic parameters.

$$\text{MRSS} = \frac{\sum_{i=1}^{N}\left(R_{\text{calc}} - R_{\text{expt}}\right)^2}{N_{\text{expt}} - N_{\text{param}}} \tag{9}$$

where N_{expt} is the number of experimental data, N_{param} is number of model parameters, R_{calc} and R_{expt} represent calculated and experimental rates, respectively. Experimental rate data are available at different temperatures, partial pressures of CO and H_2 as well as concentration of the olefin and of the catalyst (Table 3). The kinetic and equilibrium constant values can be estimated by optimizing the objective function given by the above Eq. 9 on a set of constant temperature rate data. Alternatively, a global error minimization can be done by considering all the available rate data at different temperatures and process conditions for a particular olefin. The second method is recognized as a robust technique that avoids the possible pitfalls of ending the optimization process at a local minimum. ''Temperature centering'' is a tested strategy of estimating temperature-dependent parameters by global optimization over the entire temperature range, particularly when a correlation between a rate parameter and activation energy is observed.[35–37] In this technique, the activation energy of the rate-controlling reaction step and the pre-exponential factor were obtained from the Arrhenius equation with ''temperature centering.''

$$k_i = A_i \exp\left[\frac{-E_i}{R}\left(\frac{1}{T} - \frac{1}{T_{\text{m}}}\right)\right] \tag{10}$$

Here T_{m} is introduced for temperature centering. It is usually chosen at the middle of the temperature range (it is T_{m} = 333 K in this study). An ''equilibrium constant,'' K, was similarly determined as a function of temperature using the van't Hoff equation also with temperature centering.

$$K_i^* = \exp\left[\frac{\Delta S_i}{R} - \frac{\Delta H_i}{R}\left(\frac{1}{T} - \frac{1}{T_{\text{m}}}\right)\right] \tag{11}$$

Suitable initial guess values are required for application of nonlinear regression for parameter estimation using Eq. 9 which, otherwise, may converge to local minima.[36,38] To arrive at a suitable set initial guess values for global optimization over the entire experimental temperature range, isothermal rate data at individual temperatures were first fitted and the Arrhenius plots were done to make a judgment about the

Table 3. Range of Experimental Conditions Used for Development of the Mechanistic Rate Equation

Experimental conditions	Bhanage et al.[31]	Divekar et al.[32]	Palo and Erkey[30]	Nair et al.[28]
Substrate alkene	1-Dodecene (C_{12})	1-Decene (C_{10})	1-Octene (C_8)	Styrene (C_8)
Conc. of catalyst (mol/m^3)	1.0–8.0	0–1.0	0.63–2.54	0.131–1.01
Initial conc. of 1-alkene (kmol/m^3)	0.18–2.2	0–1.0	0–1.0	0.92–6.89
P_{H2} (MPa)	0.68–1.7	0–1.38	5–13.8	1.03–4.12
P_{CO} (MPa)	0.17–2.04	0–8.11	5–13.8	0.3–4.12
T (°C)	50–70	50–70	50	60–80
Reaction volume (mL)	25	Not available	Not available	25
Solvent	Toluene	Benzene	$scCO_2$	Toluene

Table 4. Estimated M1 Kinetic Model Parameters with 95% Confidence Limits

Substrate	T (K)	k	K_1^*	K_2^*	K_3^*	K_4^*	K_5^*	*SEE*	E_a (kJ mol^{-1})
1-dodecene	323	3.1×10^4	1.24×10^3	2.5×10^5	18.0	1.5×10^4	9.0×10^5	11.5	69.7
C_{12}	333	6.0×10^4	500	1.5×10^5	5.0	1.1×10^4	4.0×10^5		*57.1[a]
	343	10.0×10^4	202	0.5×10^5	2.2	9.4×10^3	3.0×10^5		
1-decene	323	3.9×10^4	99.7	2.5×10^5	18.9	63.4	1.05×10^5	13.0	46.2
C_{10}	333	6.5×10^4	161	1.3×10^5	24.5	80.0	1.10×10^5		*49.0[b]
	343	1.1×10^5	447	8.0×10^4	33.5	93.0	1.40×10^5		
Styrene	333	4.7×10^4	13.7	3.9×10^4	5.2	3.0×10^4	2.59×10^5	2.0	63.0
C_8	343	9.8×10^4	9.0	9.0×10^2	11.4	3.5×10^4	2.65×10^5		*68.8[c]
	353	21.3×10^4	5.0	3.0×10^2	13.0	3.7×10^4	2.95×10^5		
1-octene	323	2.2×10^5	2×10^3	3.0×10^5	18.0	1.5×10^4	8.0×10^5	4.0	64.4
C_8									

initial guess and the suitability of a model. The Arrhenius parameters from these plots were then used as the starting values for an "all up" fit of rate expression. The error estimate given by Eq. 9 together with thermodynamic consistency of the calculated activation energy or negative kinetic parameter, if any, were used as the criteria of discrimination among the three macroscopic rate models.[37,39,40] Model M2 was rejected because of a high average standard error estimate ranging from 7 to 26%. Model M3 displayed a nonlinear Arrhenius plot besides a large error estimate (7 to 56%).

The rate model M1 is able to describe the experimental data reasonably well over the whole range of pressure, olefin concentration, and temperature. The estimated parameters as well as the activation energy and error estimates are presented in Table 4. These results suggest that a mechanism of reaction featuring oxidative addition of H_2 to acylrhodium intermediate species as rate determining is appropriate for describing the hydroformylation of all the substrates. Rates of hydroformylation of the olefins have been calculated for different concentrations and temperature using the generalized rate model M1 and the estimated parameters. Comparisons of these calculated values with available experimental data as well as the predictions of the empirical models reported in the literature are presented in Figures 4–6 appear to be satisfactory. Because the concentration history of 1-dodecene during hydroformylation reaction is reported by Bhanage et al.,[31] we could check the capability of the generalized model M1 to predict the concentration transient. The results presented in Figure 7 for three different temperatures further establish the accuracy of the proposed model. As a final check, we plotted the calculated and experimental rate data of all the olefins at different process conditions in the form of a parity diagram shown in Figure 8. The average prediction error is 7.6 %, whereas the maximum error is 13%. The rate parameter values were determined at 95 % confidence interval. Because the confidence interval is narrow, the sample mean may be considered to be reasonably accurate estimates of the population mean values. In addition, the values of rate parameters in the denominator of the kinetic

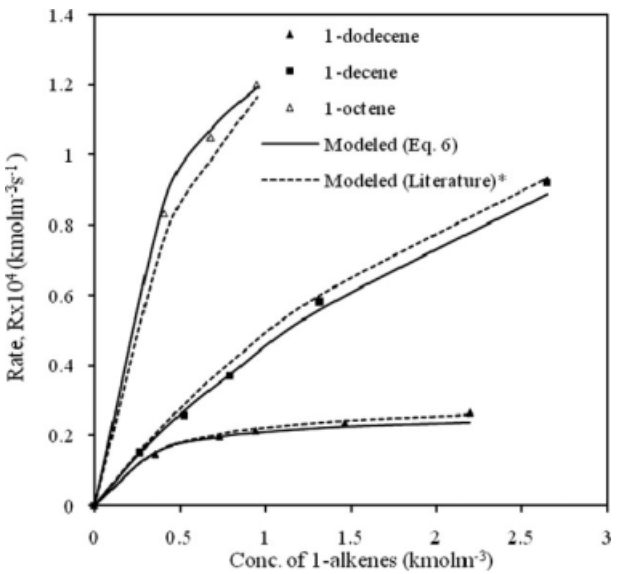

Figure 4. Experimental and predicted initial reaction rates vs. concentration of alkene, at 323 K.

*References to experimental data: 1-octene, Palo and Erkey[30]; 1-decene, Divekar et al.[32]; 1-dodecene, Bhanage et al.[31]

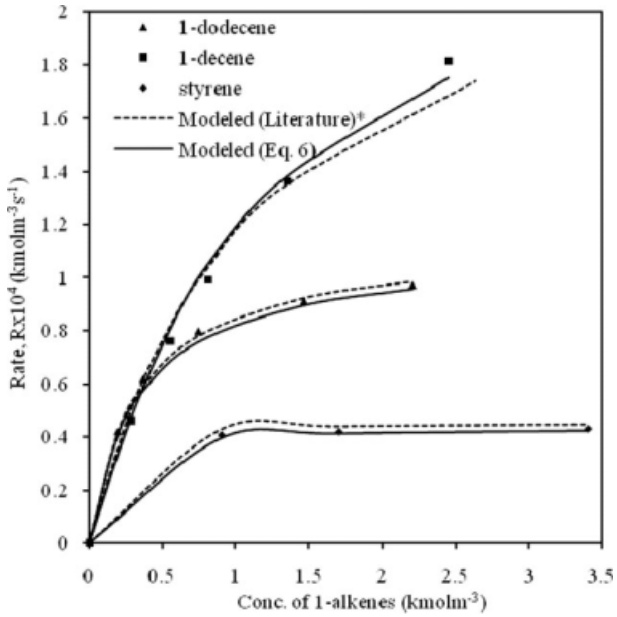

Figure 5. Experimental and predicted initial reaction rates vs. concentration of alkene at 333 K.

*References to experimental data: styrene, Nair et al.[28]; 1-decene, Divekar et al.[32]; 1-dodecene, Bhanage et al.[31]

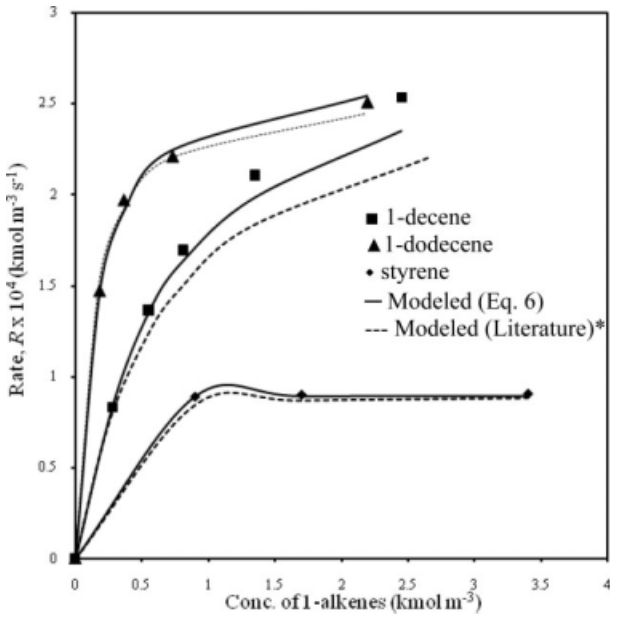

Figure 6. Experimental and predicted initial reaction rates vs. concentration of alkene at 343 K.

*References to experimental data: styrene, Nair et al.[28]; 1-decene, Divekar et al.[32]; 1-dodecene, Bhanage et al.[31]

rate expression vs. temperature (ln K vs. $1/T$) yielded good correlation (R^2) ranging from 0.97 to 0.99.

The parameters K_1^* in the denominator of Eq. 6 relate to the equilibrium constants of elementary steps in the reaction mechanism (Figure 1). The magnitudes of the parameters, that vary over a wide range, are representative of the importance of the different steps of the overall reaction. For instance, the large value of K_2^* implies that the rate of dissociation and association of ligand, step 2 and 4 are high. However, the value of K_1^* suggests that step 3 occurs at three orders of magnitude slower when compared with step 4. From the regressed value of K_4^*, the rate of the carbonyl insertion step (step 8) was found to be greater by one order of magnitude compared to the alkene insertion step. The rate constant, k, is close to the value reported by Bhanage et al.[31] Furthermore, comparing the regressed values of the rate constant, k at 333 K, the values of k increase in the order of styrene (4.7×10^4), 1-dodecene (6.0×10^4), and 1-decene (6.5×10^4) which are also supported by our calculated activation energies for H_2 oxidative addition. On the other hand, the rate constant of hydroformylation of 1-octene (2.2×10^5 at 323 K) in $scCO_2$ is found to be greatest due to the rate enhancing effect of CO_2.[41]

A negative order with respect to P_{CO} has been observed experimentally,[27,28,31,32] and therefore the concentration term of CO is expected to appear raised to a higher power in the denominator than in the numerator.[42] The regressed values of K_1^* and K_2^* for all four substrates are relatively large and suggest that the effect of the P_{CO} inhibition on the rate of reaction is highly significant. The values of K_1^* and K_2^* are larger for 1-dodecene, than for 1-decene, which in turn is larger than styrene. As P_{CO} increases, the denominator increases significantly when compared with the numerator leading to a rapid decline in the reaction rate. It is also to be noticed that at high concentration of alkene and low PPh_3 or CO concentrations leads to zero order in alkene, which has been observed experimentally for the high alkene/low PPh_3 case.[27,28,31,32]

The values of the kinetic constant for 1-dodecene was found to be 2.5 times higher than that of styrene, which confirms the good intrinsic reactivity of 1-dodecene in spite of its large molecular size. van Rooy et al.[43] also reported similar results whereby, the hydroformylation of styrene

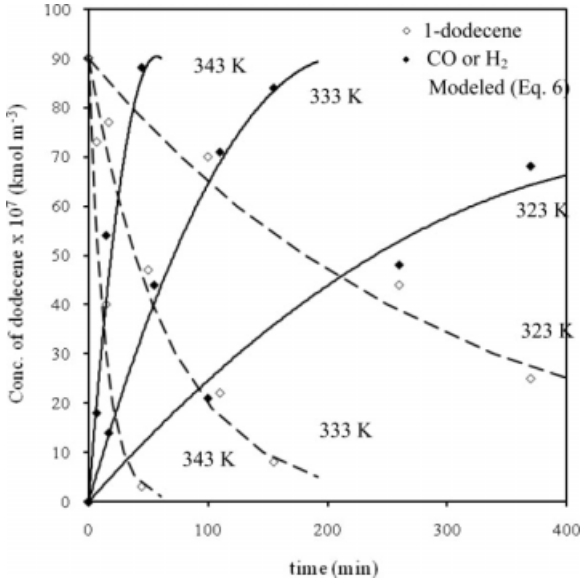

Figure 7. Experimental and predicted concentration of 1-dodecene and CO or H_2 as a function of contact time at 323, 333, and 343 K.

References to experimental data: Bhanage et al.[31]

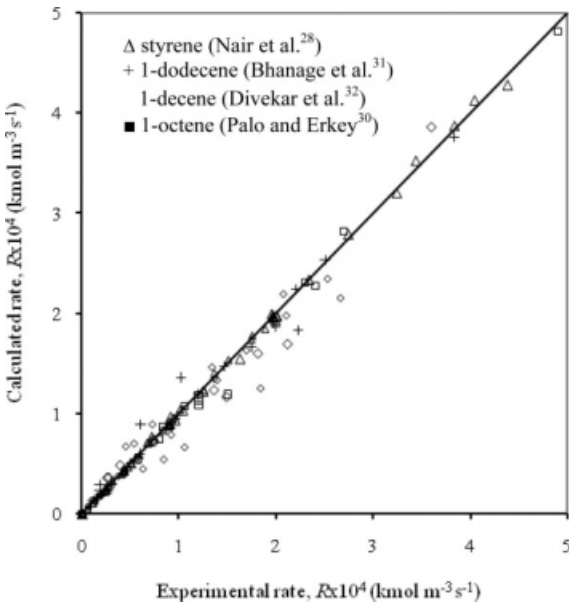

Figure 8. Parity plots of the model predictions of the rate of hydroformylation of styrene, 1-decene, and 1-dodecene in homogeneous system.

using $Rh(CO)_2(acac)$ as the catalyst precursor and tris (2-tert-butyl-4-methylphenyl) phosphite as the ligand (T = 40–100°C, P_{CO} = 2.5–44 bar, P_{H2} = 2.5–50 bar, toluene as a solvent), the rate is three times lower than that of 1-octene. For the hydroformylation of 1-dodecene, the activation energy of 57.7 kJ mol^{-1} was obtained for the rate determining step, which is close to the value of 57.10 kJ mol^{-1} reported by Bhanage et al.[31] The average deviation of predictions is 11.5%. As for 1-decene, an activation energy of 52.9 kJ mol^{-1} (for the ee species) was obtained, which is slightly higher than the value of 49.0 kJ mol^{-1} obtained by Divekar et al.[32] from their empirical model. The average deviation of prediction is 13.0%. However, the rate equation predicts the rate of hydroformylation of styrene in toluene and 1-octene in $scCO_2$ with high accuracy. An activation energy of 63.0 kJ mol^{-1} was obtained, which is lower than that obtained from the mechanistic model, (68.8 kJ mol^{-1}) reported by Nair et al.[28] The mechanistic equation reported by Nair et al.[28] was derived from the catalytic cycle described by Evans et al.[11] and the error between the predicted and experimental rate data was within ±5%. On the other hand, the predictions of the rate data by using model M1 were found to be within a maximum error of ±2.4%. The relatively small error compared with 1-dodecene and 1-decene is probably due to the presence of the aromatic ring and shorter alkyl chain of styrene. The compact molecular structure of styrene has reduced the occurrence of the isomerization reaction when compared with the long carbon chain of 1-dodecene and 1-decene. As for the rate of hydroformylation of 1-octene in $scCO_2$, the average deviation in the predicted and observed rates was found to be in the range of ±4%. This result also demonstrates that model M1 is able to predict the rate of hydroformylation of higher alkenes in both organic solvent and $scCO_2$ although several major differences exist between the conventional organic solvent-based system and the $scCO_2$ system. According to Palo and Erkey,[30] the major differences are the higher concentration of H_2 and CO in the $scCO_2$ when compared with those in organic solvent, higher total pressure of the $scCO_2$ system, and significantly different fluid densities (ρ of $scCO_2$ = 0.2–0.9 g cm^{-3}) from those of organic systems ($\rho \cong$ 0.7 g cm^{-3}).

Besides the rate-determining step of TS-3 (Figure 3) which is corroborated by experimental rate data for all the four higher alkenes, further match between the quantum chemical calculation results and the experimental data is evident from the magnitudes of the activation energies. The calculated (52.9, 57.7, and 62.2 kJ mol^{-1}) and experimental (49.2 ± 6, 57.1 ± 8, and 68.8 ± 5 kJ mol^{-1}) relative energy of the third transition structure (TS 3) and the activation energies for the hydroformylation of 1-decene, 1-dodecene, and styrene, respectively, are in reasonable agreement.[28,31,32] However, the ab initio computational approach overestimates the activation energy of the hydroformylation of 1-dodecene and 1-decene although the activation energy values are close to those obtained experimentally. The activation barrier relative to $HRh(CO)(PPh_3)_3$ catalyst is larger for styrene, than for 1-dodecene, which in turn is larger than 1-decene. This suggests that the observed reactivity seems to be influenced by the increased steric hindrance of the alkyl group of the alkene substrate.

Conclusions

Ab initio quantum chemical computations of hydroformylation of higher alkenes were performed using MP2 methodology and 6-31++G(d,p) basis set. Geometrically, optimized structures of the intermediates at transition states as well as potential energy profile of the catalytic cycles of model olefins (1-octene, 1-decene, 1-dodecene, and styrene) mediated by $HRh(CO)_2(Ph_3)_3$ complex were developed. The reaction energetics and the largest barrier of oxidative addition of H_2 were in conformity with experimental evidences and data available in the literature. Energetica of the isomers were also computed and analyzed. Generalized macroscopic rate models were developed on the basis of the catalytic reaction cycle supported by the ab initio computations. The kinetic and equilibrium parameters of the models were evaluated by nonlinear least square fitting of literature data. Correlation among the parameters was minimized by temperature centering of the Arrhenius and van't Hoff equations. Model discrimination by the conventional methodology supported the prediction of the ab initio calculation about the rate controlling step. The generalized mechanistic model predicted the reported experimental data with a better overall accuracy than the empirical models described in the literature. The average error was about 7.6% and the maximum was 13%. Thus the ab initio computational methodology is found to be a reliable tool for arriving at the reaction energetics and pathways for this class of reactions. These information together with experimental data are expected to be effective in developing macroscopic practically useful rate models.

Acknowledgments

Financial assistance from Ministry of Science, Technology, and Innovation (MOSTI), Government of Malaysia, under the Research Project No.03-02-02-SF0019: Development of a green process for the production of higher aldehydes from olefins by hydroformylation is gratefully acknowledged.

Notation

A = pre-exponential factor, units will be identical to the rate constant
ae (alternatively, 1) = the trans-isomer
[catalyst] = concentration of catalyst ($HRh(CO)(PPh_3)_3$) in the reaction mixture, kmol m^{-3}
[CO] = concentration of carbon monoxide in the reaction mixture, kmol m^{-3}
E = activation energy for rate constant, kJ mol^{-1}
ee (alternatively, 2) = the cis-isomer
ΔH = heat of reaction, kJ mol^{-1}
[H_2] = concentration of hydrogen in the reaction mixture, kmol m^{-3}
K = equilibrium constants for the elementary steps in the catalytic cycle, m^3 $kmol^{-1}$
k = reaction rate constant, units will be specific to the form of the rate expression
k^{∞} = pre-exponential rate constant, m^2 s^{-1} $kmol^{-1}$
[alkene] = concentration of alkene in the reaction mixture, kmol m^{-3}
R = gas constant, 8.314 J mol^{-1} K^{-1}
ΔS = entropy of reaction, J mol^{-1} K^{-1}
T = temperature, K

Literature Cited

1. Saeys M, Reyniers M, Thybaut JW, Neurock M, Marin GB. First-principles based kinetic model for the hydrogenation of toluene. *J Catal*. 2005;236:129–138.

2. Cavallotti C, Rota R, Faravelli T, Ranzi E. Ab initio evaluation of primary cyclo-hexane oxidation reaction rates. *Proc Combust Inst*. 2007;31:201–209.
3. Le Bris C, Defranceschi M. *Mathematical Models and Methods for Ab Initio Quantum Chemistry, Lecture Notes in Chemistry*. Vol. 74, Berlin: Springer, 2000.
4. Hehre WJ, Radom L, Schleyer PVR, Pople AJ. *Ab initio Molecular Orbital Theory*. New York: Wiley, 1986; ISBN: 9780471812418.
5. De Paz JL, Ciller J. On the use of AM1 and PM3 methods on energetic compounds. *Propellents, Explosives, Pyrotechnics*. 1993;18: 33–40.
6. Shaharun MS, Mukhtar H, Dutta BK. Solubility of carbon monoxide and hydrogen in propylene carbonate and thermomorphic multicomponent hydroformylation solvent. *Chem Eng Sci*. 2008;63:3024–3035.
7. Heil ID, Trenkle RW, Mookherje BD, Wolff RK. US Patent 4,434,086, 2000.
8. Heck RF, Breslow DS. The reaction of cobalt hydrotetracarbonyl with olefins. *J Am Chem Soc*. 1961;83:4023–4027.
9. Kiss G, Mozeleski EJ, Nadler KC, van Driessche E. Hydroformylation of ethane with triphenyl-phosphine modified rhodium catalyst. *J Mol Catal A: Chem*. 1999;138:155–176.
10. van Leeuwen PWNM, Claver C. *Rhodium Catalyzed Hydroformylation*. Dordrecht, The Netherlands: Kluwer Academic Publishers, Springer-Verlag, 2000.
11. Evans D, Osborn J, Wilkinson G. Hydroformylation of alkenes by use of rhodium complex catalysts. *J Chem Soc A*. 1968;3133–3142.
12. Saeys M, Reyniers M, Marin GB, Neurock M. Density functional theory of benzene adsorption on Pt(111). *J Phys Chem B*. 2002;106:7489–7498.
13. Zhang H, Ramachandran B, Senekowitsch J, Wyatt RE. Determination of spectroscopic constants and anharmonic force-fields for HOCl and DOCl using scaled external correlation. *J Mol Struct: THEOCHEM*. 1999;487:75–85.
14. Rocha WR, Milagre HMS, De Almeida WB. On the isomerization of β-pinene: a theoretical study. *J Mol Struct: THEOCHEM*. 2001; 544:213–220.
15. Luo X, Tang D, Li M. Quantum investigation on the mechanism of isomerization of 1-butylene catalyzed by Rh-complex. *J Mol Struct: THEOCHEM*. 2005;731:139–147.
16. Rocha WR. Hydrogen activation and aldehyde elimination promoted by homogeneous Pt-Sn catalyst: a theoretical study. *J Mol Struct: THEOCHEM*. 2004;677:133–143.
17. Schlegel HB, Yarkony DR. *Modern Electronic Structure Theory*. Singapore: World Scientific Publication, 1994:459–500.
18. Merrick JP, Moran D, Radom L. Evaluation of harmonic frequency scale factors. *J Phys Chem A*. 2007;111:11683–11700.
19. Pople JA, Schlegel HB, Krishnan R, DeFrees DJ, Binkley JS, Frisch MJ, Whiteside RA, Hout RF, Hehre WJ. Molecular-orbital studies of vibrational frequencies. *Int J Quantum Chem Quantum Chem Symp*. 1981;15:269–278.
20. Coutinho KJ, Dickson RS, Fallon GD, Jackson WR, De Simone T, Skelton BW, White AH. Isolation and characterization of hydroformylation 'intermediates' from stoichiometric reactions between phosphinoalkenes and some heterobinuclear complexes. *J Chem Soc Dalton Trans*. 1997;3193–3199.
21. Tang D, Qin S, Su Z, Hu C. Comprehensive theoretical study on the mechanism of regioselective hydroformylation of phosphinibutene catalyzed by a heterobinuclear rhodium(I)-chromium complex. *Organometallics*. 2007;26:33–47.
22. Matsubara T, Koga N, Ding Y, Musaev DG, Morokuma K. Ab initio MO study of the full cycle of olefin hydroformylation catalyzed by a rhodium complex, $RhH(CO)_2(PH_3)_2$. *Organometallics*. 1997;16: 1065–1078.
23. Musaev DG, Matsubara T, Mebel AM, Koga N, Morokuma K. Ab initio molecular orbital studies of elementary reactions and homogeneous catalytic cycles with organometallic compounds. *Pure Appl Chem*. 1995;67:257–263.
24. Brown JM, Kent AG. Structural characterisation in solution of intermediates in rhodium-catalysed hydroformylation and their interconversion pathways. *J Chem Soc Perkin Trans*. 1987;2:1597–1607.
25. Jongsma T, Challa G, van Leeuwen PWNM. A mechanistic study of rhodium tri(*o*-t-butylphenyl)phosphite complexes as hydroformylation catalysts. *Organomet Chem*. 1991;421:121–128.
26. van der Veen LA, Keeven PH, Schoemaker GC, Reek JNH, Kramer PCJ, van Leeuwen PWNM, Lutz M, Spek AL. Origin of the bite angle effect on rhodium diphosphine catalyzed hydroformylation. *Organometallics*. 2000;19:872–883.
27. van Leeuwen PWNM. *Homogeneous Catalysis, Understanding the Art*. Dordrecht, The Netherlands: Kluwer Academic Publishers, Springer-Verlag, 2004.
28. Nair VS, Mathew SP, Chaudhari RV. Kinetics of hydroformylation of styrene using homogeneous rhodium complex. *J Mol Catal A: Chem*. 1999;143:99–110.
29. Van Rooy A, de Bruijn JNH, Roobeek KF, Kamer PCJ, Van Leeuwen PWNM. Rhodium-catalysed hydroformylation of branched 1-alkenes; bulky phosphite vs. triphenylphosphine as modifying ligand. *J Organomet Chem*. 1996;507:69–73.
30. Palo DR, Erkey C. Kinetics of the homogeneous catalytic hydroformylation of 1-octene in supercritical carbon dioxide with $HRh(CO)[P(p\text{-}CF_3C_6H_4)_3]_3$. *Ind Eng Chem Res*. 1999;38:3786–3792.
31. Bhanage BM, Divekar SS, Deshpande RM, Chaudari RV. Kinetics of hydroformylation of l-dodecene using homogeneous $HRh(CO)(PPh_3)_3$ catalyst. *J Mol Catal A: Chem*. 1997;115:247–257.
32. Divekar SS, Deshpande RM, Chaudhari RV. Kinetics of hydroformylation of 1-decene using homogeneous $HRh(CO)(PPh_3)_3$ catalyst: a molecular approach. *Catal Lett*. 1993;21:191–200.
33. Deshpande RM, Chaudari RV. Kinetics of 1-hexene using homogeneous $HRh(CO)(PPh_3)_3$ complex catalyst. *Ind Eng Chem Res*. 1988; 27:1996–2002.
34. Rosales M, Duran JA, Gonzalez A, Pacheco I, Sanchez-Delgado RA. Kinetics and mechanisms of homogeneous catalytic reactions. Part 7 Hydroformylation of 1-hexene catalyzed by cationic complexes of rhodium and iridium containing PPh_3. *J Mol Catal A: Chem*. 2007;270:250–256.
35. Pant KK, Kunzru D. Catalytic pyrolysis of n-heptane: kinetic and modeling. *Ind Eng Chem Res*. 1997;36:2059–2065.
36. Wojciechowski BW, Rice NM. *Experimental Methods in Kinetic Studies*. Amsterdam: Elsevier Science BV, 2003.
37. Patel S, Pant KK. Experimental study and mechanistic kinetic modeling for selective production of hydrogen via catalytic steam reforming of methanol. *Chem Eng Sci*. 2007;62:5425–5435.
38. Routray K, Deo G. Kinetic parameter estimation for a multiresponse non-linear reaction model. *AIChE J*. 2005;51:1733–1746.
39. Pengpanich S, Meeyoo V, Rirksomboon T, Bunyakiat K. Catalytic oxidation of methane over CeO_2-ZrO_2 mixed oxide solid solution catalysts prepared via urea hydrolysis. *Appl Catal A Gen*. 2002;234: 221–233.
40. Hurtado P, Ordonez S, Sastre H, Diez FV. Development of a kinetic model for the oxidation of methane over Pd/Al_2O_3 at dry and wet conditions. *Appl Catal B Environ*. 2004;51:229–238.
41. Koeken ACJ, van Vliet MCA, van den Broeke LJP, Deelman B-J, Keurentjes JTF. Hydroformylation of 1-octene in supercritical carbon dioxide and organic solvents using trifluoromethyl-substituted triphenylphosphine ligands. *Adv Synth Catal*. 2006;348:1553–1559.
42. Helfferich FG. *Kinetics of Homogeneous Multistep Reactions*, Vol. 38. Amsterdam, Netherlands: Elsevier Science, 2001:167–168.
43. van Rooy A, Orij EN, Kamer PCJ, van Leeuwen PWNM. Hydroformylation with a rhodium/bulky phosphite modified catalyst. Catalyst comparison for oct-1-ene, cyclohexene and styrene. *Organometallics*. 1995;14:34–43.

Manuscript received Aug. 27, 2008, and revision received Mar. 18, 2009.